ELSEVIER

Materials Science and Engineering A 445–446 (2007) 364–373

MATERIALS SCIENCE & ENGINEERING A

www.elsevier.com/locate/msea

The effect of prior annealing on high temperature flow properties of and microstructural evolution in SPF grade IN718 superalloy

B.P. Kashyap [a,*], M.C. Chaturvedi [b]

[a] *Department of Metallurgical Engineering and Materials Science, Indian Institute of Technology, Mumbai 400076, Maharashtra, India*

[b] *Department of Mechanical and Manufacturing Engineering, University of Manitoba, Winnipeg, Man., Canada R3T 5V6*

Received 16 May 2006; received in revised form 8 September 2006; accepted 15 September 2006

Abstract

High temperature flow properties of superplastic forming grade IN718 superalloy, annealed at 1198–1273 K for 15 min–5 h, were investigated. Tensile specimens of grain sizes (d_o) 2.9–16.9 μm were deformed at constant strain rate of $5 \times 10^{-5}\ s^{-1}$ and by differential strain rate test technique over the strain rate range of $\sim 2.5 \times 10^{-6}$ to $3 \times 10^{-2}\ s^{-1}$ at 1198 K. The stress–strain curves exhibited flow hardening followed by flow softening. While tensile ductility was found to increase the peak stress generally decreased with the decrease in grain size. Flow hardening was attributed to concomitant grain growth in the fine-grained (d_o = 2.9–4.3 μm) samples and to deformation-induced precipitation in the coarse grained (d_o = 16.9 μm) sample. The occurrence of flow softening, in these two cases, was due to cavitation and precipitate coarsening. log(stress)–log(strain rate) curves delineated superplastic behavior with strain rate sensitivity index (m) ~0.7 and the maximum ductility was found to be 579%. However, the higher strain rates and coarser grains led to a loss of superplasticity, with $m \approx 0.2$.

Keywords: Superplasticity; IN718 superalloy; Grain growth; Cavitation; Annealing

1. Introduction

Deformation of polycrystalline materials, at high temperatures, is facilitated by grain boundary phenomena, which is recognized through the dependencies of flow stress (or strain rate) on grain size in diffusional creep and superplasticity [1]. Superplasticity, the ability of certain polycrystalline materials to exhibit tensile ductility of several hundred percent, is obtained at elevated temperatures and intermediate strain rates, when the fine and stable equiaxed grains of sizes less than 10 μm in metals and less than 1 μm in ceramics are maintained. The log–log plot of stress (σ) versus strain rate ($\dot{\varepsilon}$) exhibits a curve of sigmoidal shape, with three distinct regions [1]. The slope of this curve is known as strain rate sensitivity index (m). The values of m at low strain rates (Region I) and high strain rates (Region III) are known to be equal to or less than 0.3 and 0.2, respectively. The intermediate region of strain rates (Region II), where m is found to be greater than 0.3, is called superplastic region. During superplastic deformation, the effect of grain size (d) on strain rate, at the given temperature (T, absolute) and flow stress, can be expressed as

$$\dot{\varepsilon} = \frac{K}{d^p} \tag{1}$$

where K is a proportionality constant and p is the exponent of inverse grain size. The values of p are generally found to lie between 2 and 3. However, there appeared a significant deviation in the values of p in some superplastic materials [2]. While the stable and fine equiaxed grains for exhibiting superplasticity are achieved by nearly equi-partitioning of the constituent phases in two-phase materials, the same in quasi-single phase is obtained by grain boundary pinning by the dispersed small particles. The distributions of such dispersoids, along with the kind of microstructures developed through new thermo-mechanical processing for superplasticity (e.g. ref. [3]), restrict the operation of main mechanism for superplastic deformation, viz. the grain boundary sliding (GBS). As compared to the large contributions of GBS (exceeding 50% of total strain) during superplastic deformation of several materials [4], only limited

* Corresponding author. Tel.: +91 2225767622; fax: +91 2225723480.
E-mail address: bpk@iitb.ac.in (B.P. Kashyap).

0921-5093/$ – see front matter © 2006 Elsevier B.V. All rights reserved.
doi:10.1016/j.msea.2006.09.053

GBS but largely the dislocation slip mechanism is reported to contribute to superplastic deformation in some quasi-single phase materials [5,6]. Such materials, containing dispersoids, add to new microstructural features, which limit grain boundary phenomena and act as sites for stress concentration. In spite of this, the maximum superplasticity reported in such materials is not inferior to what is known in other two-phase materials. However, not much work seems to have been reported to show the effect of grain size on flow behavior in such superplastic materials.

Recently, IN718 superalloy was reported [7–10] to exhibit superplasticity. The superplastic forming (SPF) grade IN718 superalloy was found to contain a large volume fraction of precipitates and the microstructure in as-processed state possessed banded but very fine grains [10]. To our knowledge, results of a systematic study of the effect of annealing or grain size on superplastic behavior of this material have not been reported. Therefore, the aim of present work was to examine the effect of prior annealing on superplastic properties of IN718 superalloy, which contains fine grains as well as precipitates.

2. Experimental procedure

The SPF grade IN718 superalloy was obtained in the form of a sheet of 1.3 mm thickness. The chemical composition (wt.%) was analyzed to be Ni–17.4Cr–19.4Fe–4.99Nb–3.11Mo–1.07Ti–0.48Al–0.034C–0.19Cu. Metallographic samples were mechanically polished, with Leco colloidal silica at the final stage. Electrolytic etching was done at room temperature in a solution of 10 g oxalic acid in 90 ml water at an applied potential of 6 V. Microstructure for cavitation was examined in as-polished condition whereas the same for grain structure was examined after etching. Grain size (mean intercept length) was measured manually by mean linear intercept method employed directly to the images of the samples being examined under microscope. More than 500 intercepts were counted to determine the grain size of each specimen. TEM specimens were spark-cut into 3 mm discs from the mechanically thinned sheet, which was followed by further mechanical thinning and electropolishing. The electrolyte used was a mixture of 15% perchloric acid in 85% methanol and the condition employed for electrothinning was $T = 233$ K and applied voltage of 18 V. The specimens were examined in JEOL 2000FX TEM/STEM operating at 200 kV.

Two sets of tensile specimens of gage lengths 10 and 20 mm, but of the same gage width of 5.4 mm, were machined. These, along with the representative metallographic samples, were annealed in a tubular furnace at selected temperatures within an accuracy of ±3 K. Tensile tests were conducted in air by computer interfaced Instron universal testing machine. Duration of 20 min was given for heating to and soaking at the test temperature, prior to tensile tests. Test temperatures were controlled within an accuracy of ±1 K. Tensile specimens of 10 mm gage length were deformed at constant true strain rates whereas the specimens of 20 mm gage length were used for differential strain rate tests.

3. Results and discussion

3.1. Annealed microstructure

The as-received sheet had a banded microstructure with relatively coarser grain sizes in the rolling surface and very fine grain sizes in the longitudinal and transverse surfaces. This aspect of the material was presented and discussed earlier [10]. TEM examination delineated very fine precipitates at grain boundaries, triple points and in grain interior. This is shown by a bright field image along with a diffraction pattern of the largest precipitate in Fig. 1a and b. Given in Fig. 1c and d are the EDAX

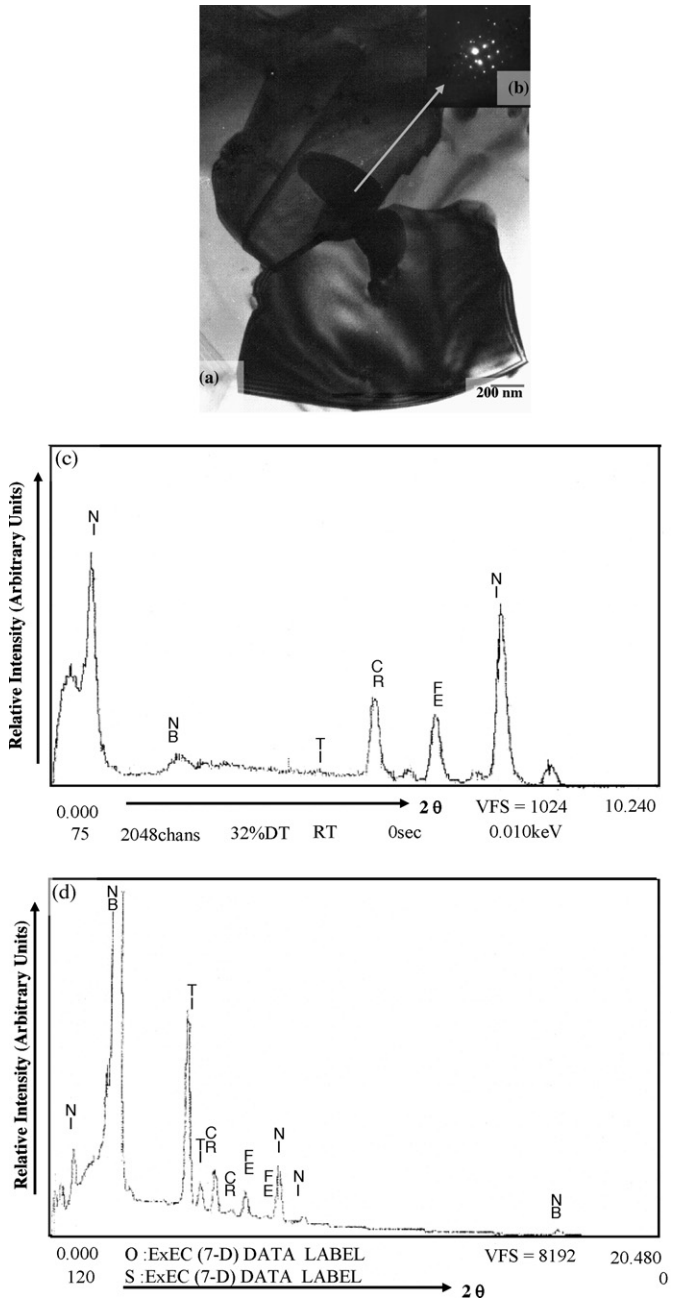

Fig. 1. (a) TEM micrograph showing the presence of precipitates in as-received sheet, (b) diffraction pattern of the largest precipitate present at triple point, (c) EDAX spectrum of matrix and (d) EDAX spectrum of precipitate.

Table 1
Compositions (at.%) of matrix and precipitates in the as-received IN718 superalloy

Element	Matrix	Precipitate
Fe	18.47	5.95
Cr	20.72	5.99
Nb	3.30	17.87
Mo	2.50	1.57
Ni	52.56	63.45
Al	0.65	0.60
Si	0.64	1.39
Mn	0.28	0.00
Ti	0.89	3.18

spectrum of the matrix and precipitate in as-received condition. The respective chemical compositions are listed in Table 1. Based on the chemical composition and its comparison with that given in literature [11,12], the precipitates were identified to be BCT-γ'' phase.

Annealing was done in the temperature range of 1198–1273 K for 15 min–5 h with a purpose of producing different grain sizes. The annealing conditions and the resulting grain sizes are presented in Table 2. Shown in Fig. 2a–c are the three microstructures—first in as-received condition (Fig. 2a), second developed upon annealing for 5 h at 1198 K (Fig. 2b) and the third developed upon annealing for 15 min at 1273 K (Fig. 2c). As described earlier [10], the microstructure of the as-received sheet was banded and inhomogeneous. However, annealing led to homogenization of microstructure, with no significant difference in the microstructures of the three orthogonal surfaces of the material. Upon annealing within the temperature range of 1198–1248 K, the grains remained fine but with much reduced banding. However, some bi-modal distributions of grain sizes were noticed to develop. For example, upon annealing at 1223 K for 1 h, the grain sizes of 3.5 and 5.2 μm were obtained in the regions of relatively finer and coarser microstructures, respectively. Annealing at 1273 K was found to result in coarse equiaxed grains within a short annealing time of 15 min. Similar effect was noted on annealing for still shorter time of 30 s and even at lower temperature of 1258 K (not included here). The precipitates were also examined qualitatively at higher magnifications. A large amount of precipitates were found to remain upon annealing up to the temperature of 1248 K whereas an

Table 2
Effect of annealing condition on grain size of SPF grade IN718 superalloy

Condition (T, K/t, h)	1198/5	1223/1	1248/0.25	1248/4	1273/0.25
Grain size (μm)	2.9	3.5	3.7	4.3	16.9

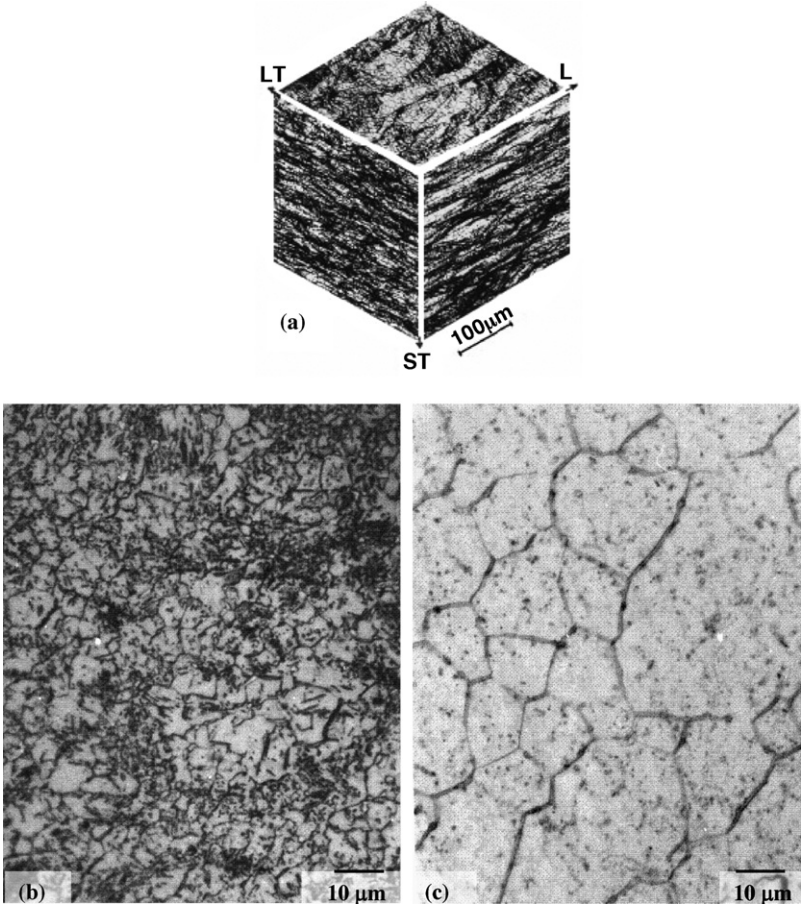

Fig. 2. Microstructures of SPF grade IN718 superalloy in: (a) as-received condition and (b and c) upon annealing (temperature/time); (b) 1198 K/5 h and (c) 1273 K/15 min.

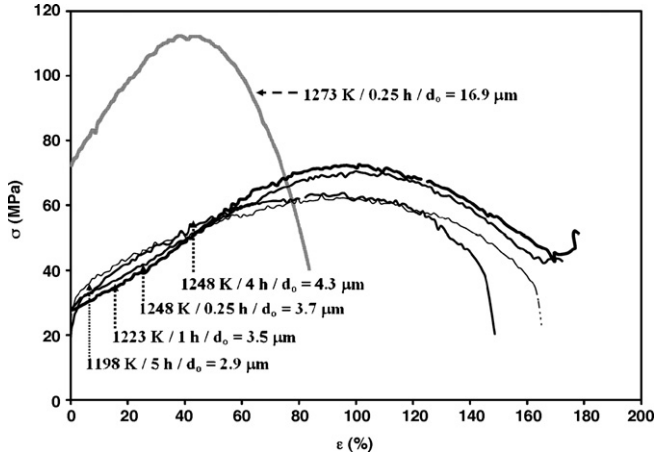

Fig. 3. True stress–true strain curves of SPF grade IN718 superalloy annealed (temperature (T), time (t) and grain size (d_o) being shown along with the curves) at various conditions. (Deformed at $T = 1198$ K, $\dot{\varepsilon} = 5 \times 10^{-5}$ s^{-1}.)

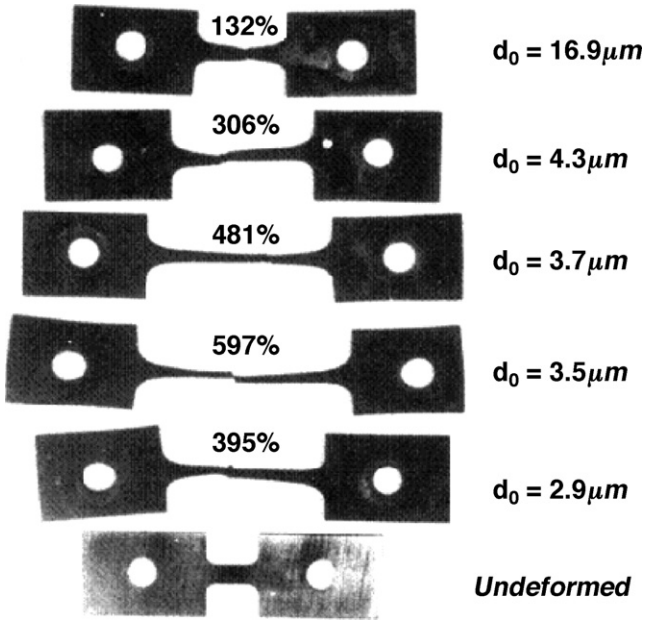

Fig. 4. Silhouettes of tensile specimens deformed to failure at $T = 1198$ K, $\dot{\varepsilon} = 5 \times 10^{-5}$ s^{-1}.

increase of only 10 K in annealing temperature (i.e. annealing at 1258 K) resulted in an almost precipitate-free clean microstructure. The retention of very fine grains and the existence of precipitates, up to the annealing temperature of 1248 K, suggest that grain growth was suppressed through pinning of grain boundaries by the precipitates. No work was undertaken in this study to determine the solvus line above that the dissolution of precipitates could occur. But, the qualitative microstructural examination suggested it to lie somewhere between 1248 and 1258 K.

3.2. Flow behavior

Tensile specimens, annealed as shown in Table 2, were deformed by constant strain rate and differential strain rate test techniques at $T = 1198$ K. Presented below is the flow behavior obtained in these two cases.

3.2.1. Stress–strain behavior

Constant strain rate tests were performed up to failure at $\dot{\varepsilon} = 5 \times 10^{-5}$ s^{-1}. The resulting stress (σ)–strain (ε) curves are presented in Fig. 3 and the silhouettes of deformed tensile specimens are shown in Fig. 4. While the σ–ε curve for the specimen of $d_o = 16.9$ μm, annealed at 1273 K for 15 min, shows distinctly the maximum flow stress and the minimum ductility; the specimens annealed at other conditions show overlapping flow stresses in the early part of the deformation and significant difference in flow stresses at later part of deformation only. The values of tensile ductility are also noted to be significantly different for specimens annealed at different conditions. Within the range of grain sizes investigated, the flow stress is noticed to increase whereas ductility is noticed to decrease with the increase in grain size. The plot of ductility as a function of grain size is given in Fig. 5a. Fig. 5b shows the plot of peak stress as a function of grain size. The strains, corresponding to the peak stresses, were also plotted (not shown here) as a function of grain size, which like ductility, decreased with the increase in grain size. The log–log plot of peak stress (σ_p) versus grain size (d_o) suggested a relationship of the type:

$$\log(\sigma_p) = 3.35 \log(d_o) + 55.48 \quad (R^2 = 0.95) \tag{2}$$

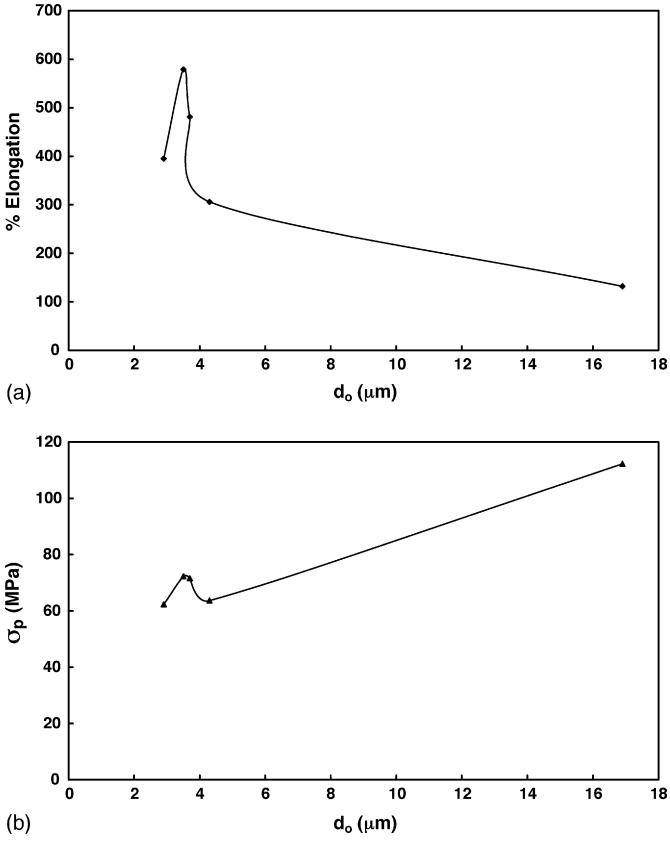

Fig. 5. Plot of: (a) maximum elongation at failure and (b) peak stress (σ_p) as a function of initial grain size (d_o) ($T = 1198$ K, $\dot{\varepsilon} = 5 \times 10^{-5}$ s^{-1}).

where R^2 is the regression coefficient of a linear fit. From the constitutive relationship for high temperature deformation [1], the slope of log(stress) plot versus log(grain size) plot represents the value of p/n (n being the stress exponent), which is estimated to be 3.35 here.

The stress–strain curves in Fig. 3 first show flow hardening, reaching the peak stresses, which is followed by flow softening. The flow hardening rate is noticed to be highest in the specimen of the largest grain size ($d_o = 16.9\ \mu m$). Some specimens of smaller grain sizes also tend to exhibit a second stage of flow hardening just before failure. Such upward rise in flow stress is known [13] to occur in cavitating superplastic materials by virtue of microtensile specimens (and so the locally higher strain rate of deformation, for a given external strain rate) being created between large cavities at coalescence stage.

3.2.2. Stress–strain rate behavior

Tensile specimens were deformed by differential strain rate test technique over the strain rate range of $\sim 2.5 \times 10^{-6}$ to $2 \times 10^{-2}\ s^{-1}$. Prior to following the sequence from the lowest towards the highest strain rates, the same specimens were deformed at an intermediate strain rate of $\sim 5 \times 10^{-4}\ s^{-1}$. The reasons for this prestraining are two-fold. Firstly, the specimen deformed at this strain rate and subsequently changed to the lowest stain rate of $\sim 2.5 \times 10^{-6}\ s^{-1}$ picks up the load without undergoing relaxation at latter strain rate, whereby the time required at such a low strain rate is minimized. Secondly, the repetition of strain rate $\sim 5 \times 10^{-4}\ s^{-1}$ in the beginning of the differential strain rate test and on subsequent ascending order of the differential strain rate test provides a means to examine whether there occurs flow hardening or flow softening during intermediate deformation at the various strain rates and strain involved [10]. This whole sequence of strain rate changes, typically, $\dot{\varepsilon}_1 = 5 \times 10^{-4}\ s^{-1}$, $\dot{\varepsilon}_2 = 2.5 \times 10^{-6}\ s^{-1}$, $\dot{\varepsilon}_3 = 5 \times 10^{-6}\ s^{-1}$, $\dot{\varepsilon}_4 = 1 \times 10^{-5}\ s^{-1}$, $\dot{\varepsilon}_5 = 2 \times 10^{-5}\ s^{-1}$, $\dot{\varepsilon}_6 = 5 \times 10^{-5}\ s^{-1}$, $\dot{\varepsilon}_7 = 1 \times 10^{-4}\ s^{-1}$, $\dot{\varepsilon}_8 = 2 \times 10^{-4}\ s^{-1}$, $\dot{\varepsilon}_9 = 5 \times 10^{-4}\ s^{-1}$, $\dot{\varepsilon}_{10} = 1 \times 10^{-3}\ s^{-1}$, $\dot{\varepsilon}_{11} = 2 \times 10^{-3}\ s^{-1}$, $\dot{\varepsilon}_{12} = 5 \times 10^{-3}\ s^{-1}$, $\dot{\varepsilon}_{13} = 1 \times 10^{-2}\ s^{-1}$ and $\dot{\varepsilon}_{14} = 2 \times 10^{-2}\ s^{-1}$, i.e. starting from the first strain rate of $\sim 5 \times 10^{-4}\ s^{-1}$, employed also for pre-straining, and ending at the highest strain rate of $\sim 2 \times 10^{-2}\ s^{-1}$, will be referred to as one cycle. It may be noted that the strain rates mentioned here are approximates, as the gage length of the tensile sample itself increased continuously during deformation and no adjustment was made in the cross-head speeds for repeating exactly the same strain rates subsequently. Such differential strain rate testing was repeated to collect $\sigma - \dot{\varepsilon}$ data up to three cycles from the same specimen, which are identified as cycle 1, cycle 2 and cycle 3, respectively. These three cycles are schematically illustrated as inset in Fig. 6a. $\ln(\sigma)$–$\ln(\dot{\varepsilon})$ plot for different cycles were observed to be comparable, except some indication of flow softening exhibited by the curve belonging to cycle 3. A typical plot of $\ln(\sigma)$–$\ln(\dot{\varepsilon})$ data for the three cycles, obtained from the specimen annealed at 1223 K for 1 h are shown in Fig. 6a. The slope of the curve (m) is greater at lower strain rates and is smaller at the higher strain rates. The values of m obtained from the load-extension curves of differential strain rate tests, and by using the following equation, are plotted as a function of strain rate in Fig. 6b.

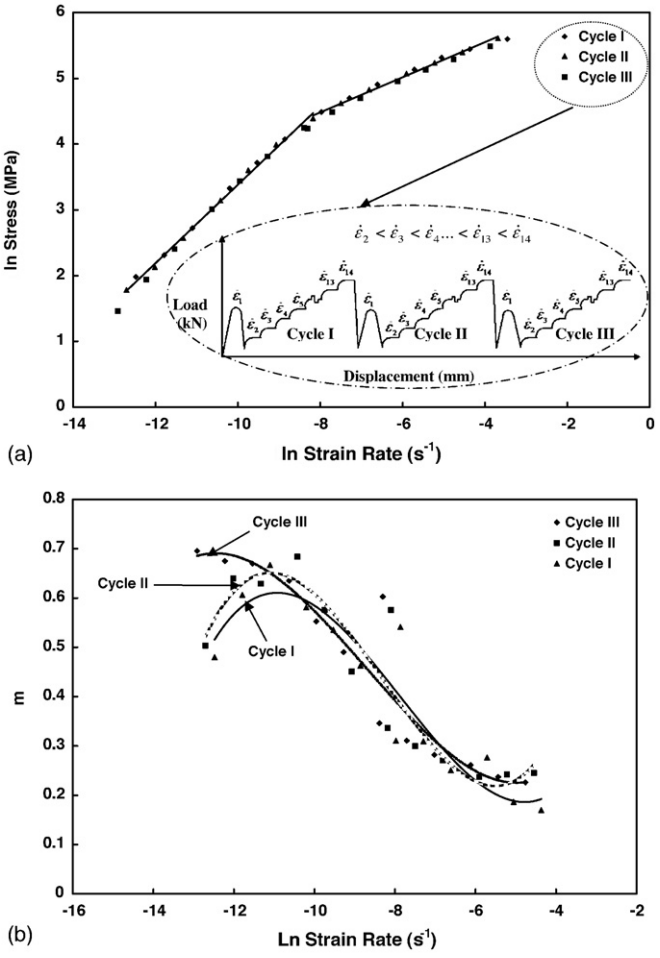

Fig. 6. (a) Plot of $\ln(\sigma)$ vs. $\ln(\dot{\varepsilon})$ ($T = 1198$ K, $d_o = 2.9\ \mu m$) from three cycles of differential strain rate tests. Inset schematically illustrates the three cycles of strain rate changes performed. Each cycle consisted of the following sequence of strain rates: $\dot{\varepsilon}_1 = 5 \times 10^{-4}\ s^{-1}$, $\dot{\varepsilon}_2 = 2.5 \times 10^{-6}\ s^{-1}$, $\dot{\varepsilon}_3 = 5 \times 10^{-6}\ s^{-1}$, $\dot{\varepsilon}_4 = 1 \times 10^{-5}\ s^{-1}$, $\dot{\varepsilon}_5 = 2 \times 10^{-5}\ s^{-1}$, $\dot{\varepsilon}_6 = 5 \times 10^{-5}\ s^{-1}$, $\dot{\varepsilon}_7 = 1 \times 10^{-4}\ s^{-1}$, $\dot{\varepsilon}_8 = 2 \times 10^{-4}\ s^{-1}$, $\dot{\varepsilon}_9 = 5 \times 10^{-4}\ s^{-1}$, $\dot{\varepsilon}_{10} = 1 \times 10^{-3}\ s^{-1}$, $\dot{\varepsilon}_{11} = 2 \times 10^{-3}\ s^{-1}$, $\dot{\varepsilon}_{12} = 5 \times 10^{-3}\ s^{-1}$, $\dot{\varepsilon}_{13} = 1 \times 10^{-2}\ s^{-1}$ and $\dot{\varepsilon}_{14} = 2 \times 10^{-2}\ s^{-1}$. (b) Plot of m vs. $\log(\dot{\varepsilon})$ from three cycles of differential strain rate tests ($T = 1198$ K, $d_o = 2.9\ \mu m$) described in (a).

$$m = \ln\left(\frac{p_2}{p_1}\right) \Big/ \ln\left(\frac{v_2}{v_1}\right) \tag{3}$$

Here p and v represent the peak load and the corresponding cross-head speed, respectively, and the subscripts 1 and 2 represent the two adjoining sets of p and v values in the differential strain rate tests. The maximum values of $m \approx 0.7$ were determined towards the lower strain rate range. Towards the highest strain rates the values of m were determined to be as low as 0.2. The higher values of m are typical of superplastic behavior, which is distinguished [1] on the basis of m being greater than 0.3 but more often around 0.5. The lower values of m at the strain rates of $\sim 7 \times 10^{-4}\ s^{-1}$ and above ($m < 0.3$) suggest the deformation to be controlled by dislocation climb creep, which predicts the value of m to be 0.20–0.25 ($n = 1/m = 4$–5) [1].

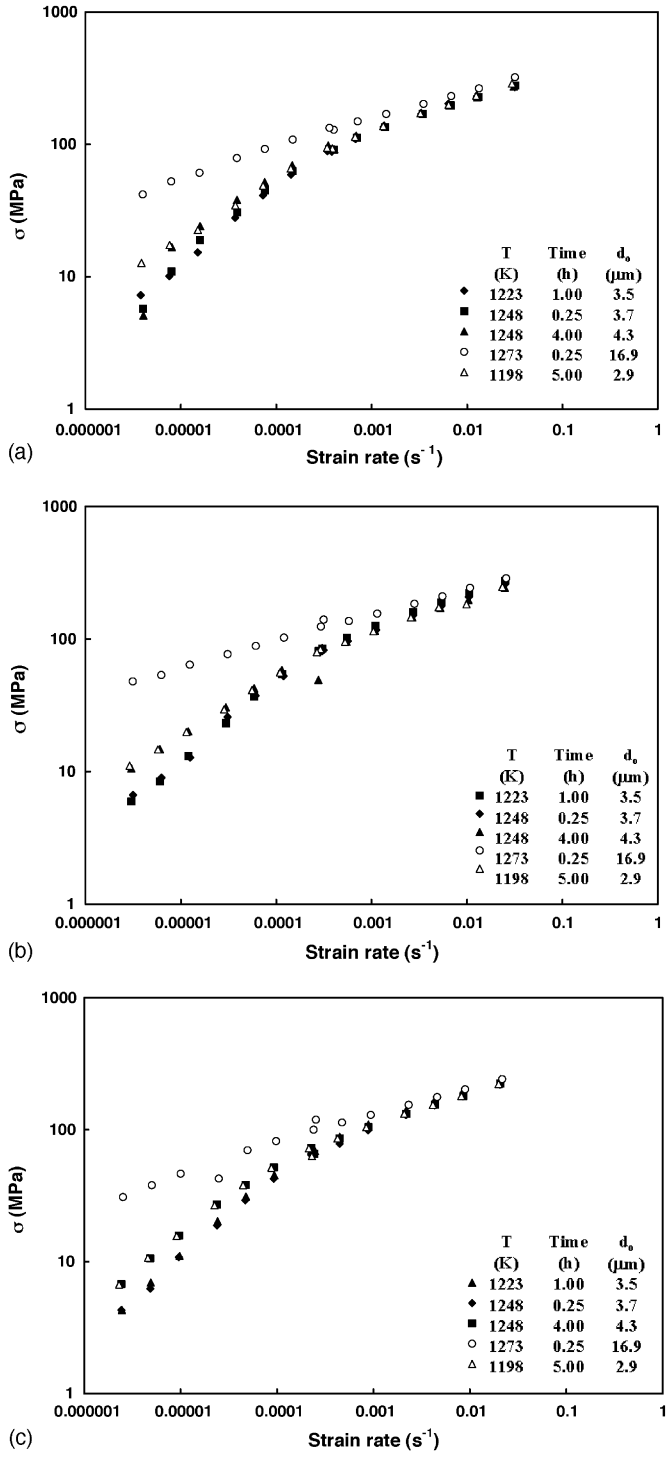

Fig. 7. log(σ) vs. log($\dot{\varepsilon}$) plot for specimens of different annealing conditions (initial grain sizes): (a) cycle I, (b) cycle II and (c) cycle III.

log(σ)– log($\dot{\varepsilon}$) plot for different grain sizes are presented in Fig. 7a–c for various cycles. While the specimen annealed at 1273 K for 15 min shows lower slope (m) over the entire strain rate range investigated, greater slope at lower strain rates and smaller slope at higher strain rates were distinctly observed in specimen annealed under different conditions. These behaviors also support superplastic mechanism of deformation at lower strain rates and dislocation climb creep mechanism at higher strain rates. However, for the specimen annealed at 1273 K (d_o = 16.9 μm), deformation is suggested to occur by dislocation climb mechanism over the entire range of strain rates. As the grain size increases, the strain rate range describing the superplastic region (Region II) shifts towards lower strain rates and Region III behavior (m < 0.3) of usually higher strain rates expands over a larger strain rate range [1]. This is suggested to be the reason that only Region III behavior is seen in the specimen of grain size 16.9 μm. A comparison of log(σ)– log($\dot{\varepsilon}$) curves for different grain sizes also delineates some effect of grain size on flow behavior in superplastic region but not so distinct in Region III. A comparison of log(σ)– log($\dot{\varepsilon}$) curves of cycles I, II and III, within the superplastic region, shows that the spread in flow stress for different grain sizes decreases with the increasing number of cycles. This behavior may be associated with the variation in the nature of microstructural evolution and its influence on flow hardening and flow softening for the specimens of different initial grain sizes. The variation in m as a function of strain rate for various annealing conditions is shown in Fig. 8a–c. In conformity with the log(σ)– log($\dot{\varepsilon}$) plot, the values of m for the fine grained specimens are found to be much larger than that obtained from the specimen of grain size 16.9 μm at lower strain rates, but not so at higher strain rates. In some cases, the values of m are noticed to increase or decrease with the increasing number of cycling (especially, compare the peak values of m in Fig. 8). This is also attributed to microstructural evolution during superplastic deformation.

3.3. Microstructural evolution

Tensile specimens deformed to failure were examined for cavitation and grain structure developing during high temperature deformation. The microstructures of the shoulder and gage sections of the two tensile specimens, whose initial microstructures are shown in Fig. 2b and c, are presented in Fig. 9a–d. The following changes in microstructures are noted by comparing the initial microstructures (Fig. 2a–c), the microstructures in shoulder sections (Fig. 9a and c), which involve the effects of time and test temperature, and the microstructures in gage sections (Fig. 9b and d) which, in addition, undergo plastic deformation. (i) There occurred grain growth in both the shoulder and gage sections but the grain size in the latter was greater. (ii) With respect to the as-received microstructure, annealing at 1273 K for 15 min exhibited grain growth and dissolution of precipitates. But, when the tensile specimen annealed under this condition was subjected to straining, the shoulder and gage sections exhibited further grain growth. Not only this but also there appeared significantly larger volume fraction of precipitates in the gage section of this specimen, whose morphology was noticed to be different from that of the as-received, as-annealed as well as the shoulder samples. The larger grain size in the gage section, than that present in the shoulder, was reviewed [4] in a number of superplastic materials. The enhanced grain growth during superplastic deformation was attributed [14] to grain boundary migration induced by the stress concentration arising from grain boundary sliding. The precipitates, shown in Fig. 9d, are different from the initial precipitates present in the

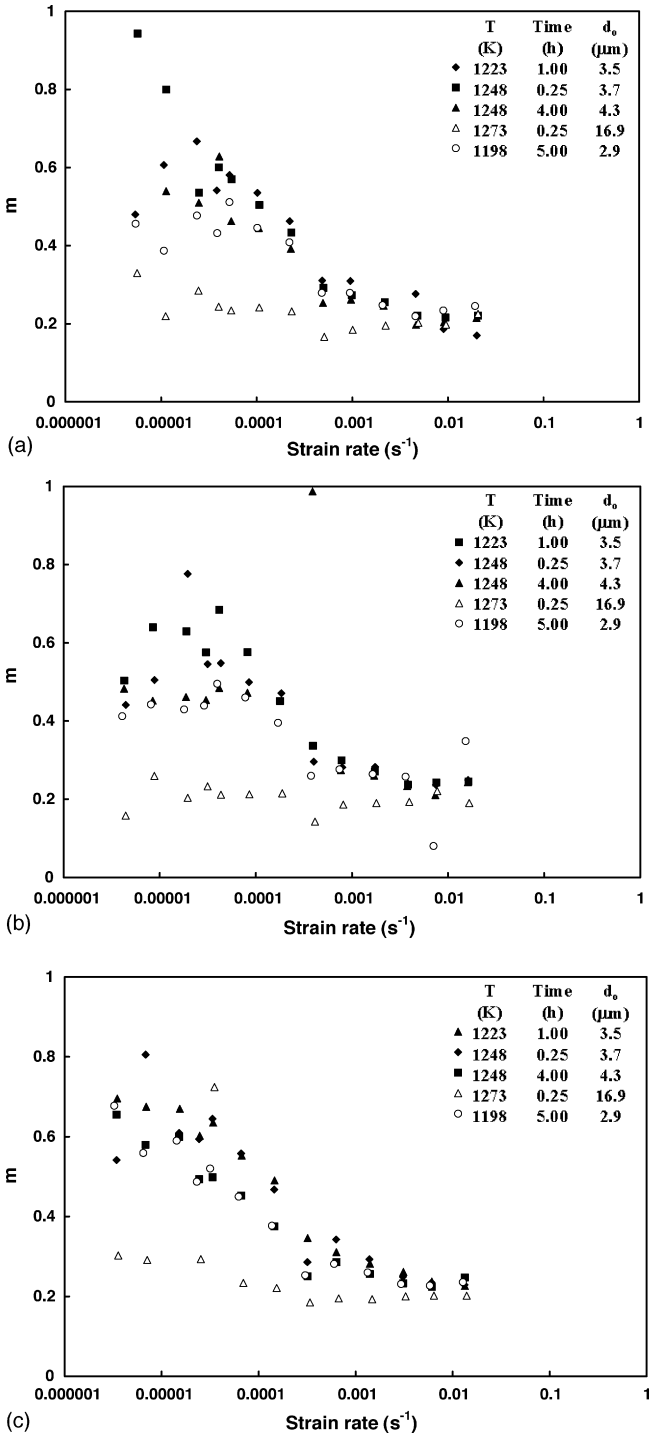

Fig. 8. m vs. $\log(\dot{\varepsilon})$ plot for specimens of different annealing conditions (initial grain sizes): (a) cycle I, (b) cycle II and (c) cycle III.

as-received sheet. The precipitates in the gage section are similar to those that were obtained by static annealing at much higher temperature ($T \geq 1373$ K). Such precipitates in IN718 superalloy were identified to be carbides. This is also supported by the TTP (temperature–time–precipitation) curves for different precipitates in the IN718 superalloy [15]. The appearance of these precipitates in the gage section and their near absence in the shoulder section suggest that the precipitation process is favored by deformation mechanism. Under the present test condition ($T = 1198$ K, $\dot{\varepsilon} = 5 \times 10^{-5}\ s^{-1}$ and $d_o = 16.9$ μm), deformation is suggested to be by dislocation climb creep. Therefore, the enhancement of precipitation may be related to the presence of dislocations and their activity during high temperature deformation. While grain coarsening during superplastic deformation has been extensively analyzed [14,16], no systematic analysis of precipitate coarsening seems to be reported in the superplastic literature. However, static grain growth in the two-phase materials has revealed that both the phases, viz. the matrix and the second phase (equivalent to particles), undergo coarsening following the Zener type relationship [17,18]. In spite of the difference in the kinetics of grain coarsening [19] in the materials containing particles ($d_m \propto t^{1/3}$, where d_m is the grain size of matrix at annealing time of t) and massive two phases ($d_m \propto t^{1/4}$), Seidensticker and Mayo [16] found that normalized grain growth rate ($\dot{d}$) during superplastic deformation increases with strain rate ($\dot{d} \propto \dot{\varepsilon}$) not only in metals but also in ceramics. Accordingly, one would expect the rate of particle coarsening to increase with increasing strain rate during superplastic deformation. This aspect of microstructural changes during superplastic deformation opens up an interesting avenue for further study.

Another noticeable microstructural change, during high temperature deformation, is the occurrence of cavitation. Qualitatively, more cavities were formed during superplastic deformation and only limited cavities were observed under non-superplastic condition. The cavity micrographs of the specimens deformed under superplastic conditions are illustrated in Fig. 10a–c and that of the specimen deformed under non-superplastic condition is illustrated in Fig. 10d. The large number of cavities seen in superplastically deformed specimens may be a result of stress concentration developed by grain boundary sliding and its inadequate accommodation. In spite of the large number of cavities present in superplastically deformed samples, the elongations at failure were quite large (306–579%). Such effects, of maximum cavitation during superplastic deformation and minimum cavitation when deformed under non-superplastic condition, were reported in some other superplastic materials as well [13]. It is possible that the cavities remain separated and do not undergo further growth and coalescence due to grain rotation and grain switching, which follow grain boundary sliding during superplastic deformation.

3.4. Effect of microstructure on flow behavior

All of the stress–strain curves in Fig. 3 exhibit flow hardening in the early part of the deformation. The measurement of terminal grain sizes supported the occurrence of grain growth. The grain growth (normalized by ductility, viz. $(d_g - d_o)/\varepsilon_f$), where d_g is the grain size in gage section upon failure at true strain of ε_f and d_o is the initial grain size) was determined to range from 0.4 to 16.3 μm per unit strain. The flow hardening may be partly due to such grain growth. However, it is interesting to note that the tensile specimen annealed at 1273 K for 15 min had initial coarse grain size of 16.9 μm and, accordingly, it did not show superplastic behavior as noted from the $\log(\sigma)$–$\log(\dot{\varepsilon})$ plot in Fig. 7. In spite of the dislocation based creep deformation

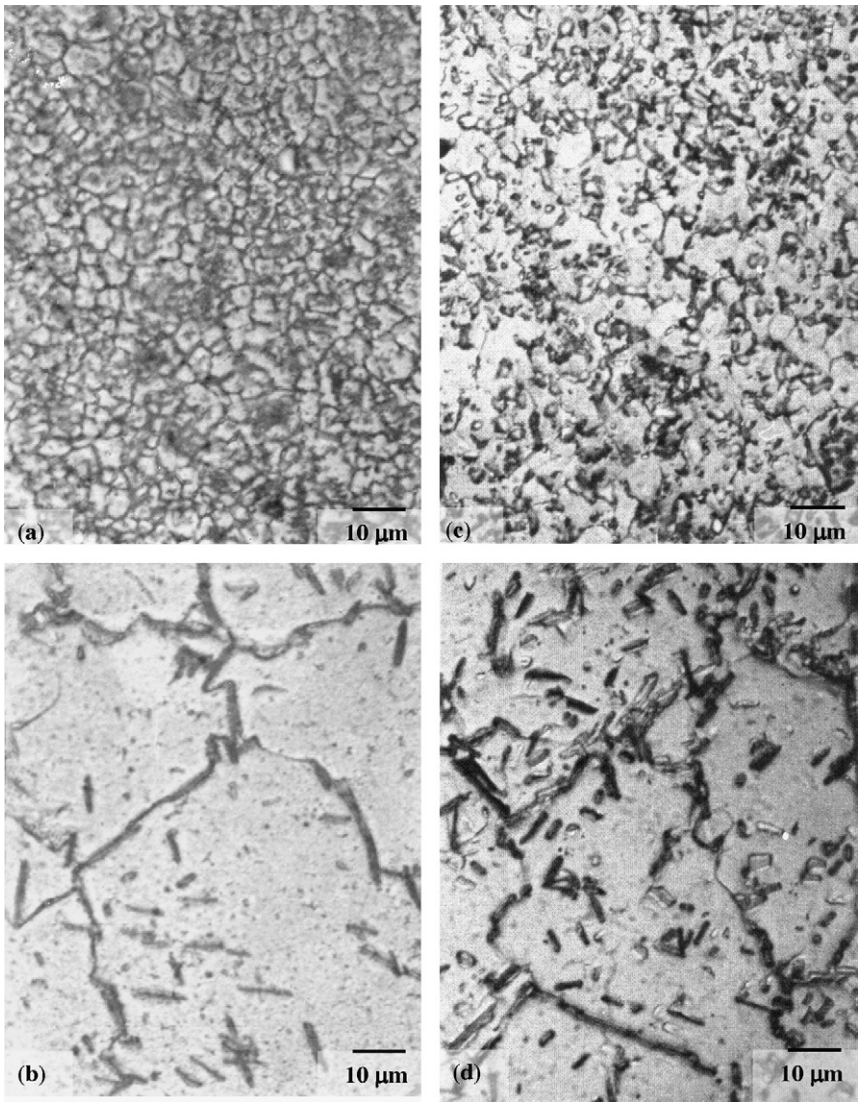

Fig. 9. Microstructures developed in the shoulder (a and c) and gage (b and d) sections of the specimens deformed to failure. (a and b) Shoulder and gage of tensile specimen annealed at 1198 K/5 h (Fig. 2a, the initial microstructure). (c and d) Shoulder and gage of tensile specimen annealed at 1273 K/15 min (Fig. 2b, the initial microstructure).

mechanism of Region III, there occurred substantial flow hardening as seen in Fig. 3. This flow hardening may be attributed to dislocation–precipitate interactions rather than that associated with grain growth, as the microstructure upon deformation of this specimen is seen to contain precipitates.

The effect of grain size on flow properties during superplastic deformation is not brought out clearly in Figs. 3 and 7. An attempt to evaluate the effect of grain size (figures not being presented here) within superplastic region suggested the value of p/n to be 0.91 with a very poor fit of $\log(\sigma)$–$\log(d)$ plot. According to this, if $m = 0.5$ (as suggested by Fig. 7 at $\dot{\varepsilon} = 1 \times 10^{-5}\ s^{-1}$), the value of p is found to be 0.46, which is much smaller than that known for superplastic deformation ($p = 2$–3). However, if no distinction is made between deformation mechanisms in fine grained and coarse-grained materials, but rather a comparison is made at a constant strain rate of deformation, then a significant effect of grain size on peak stress emerges as suggested by Fig. 5b.

Subsequent to attaining the peak stresses, the stress–strain curves, corresponding to all the specimens, exhibit flow softening to a varying extent (Fig. 3). The fine-grained specimens were found to exhibit cavities, which can contribute to such flow softening once the effect of cavitation dominates over the effect of concurrent grain growth. However, the coarse-grained specimen also exhibited flow softening despite the much lower level of cavities seen upon deformation. During high temperature deformation, the flow hardening with decreasing work hardening rate in the early part of deformation is ascribed to dynamic recovery whereas the subsequent softening is ascribed to dynamic recrystallization [20]. Since no dynamic recrystallization was noticed to occur in this study, the source of flow softening cannot be related to concurrent grain size either. It is possible that precipitation, which was responsible for flow hardening in the beginning, also became the source of flow softening subsequently because the coarsening of the precipitates during overaging leads to a decrease in hardness. Although, based on the lower values of

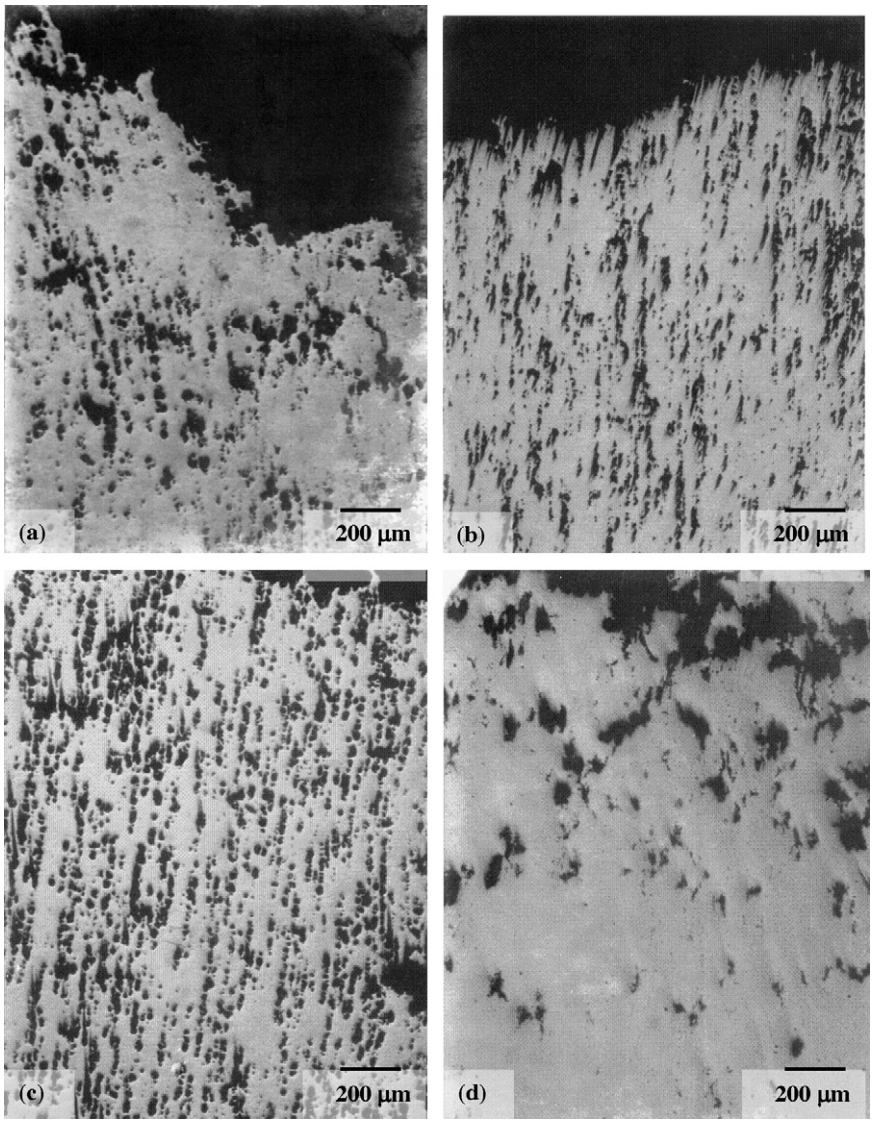

Fig. 10. Development of cavities upon failure of the tensile specimens pre-annealed under various conditions (T, K/t, h): (a) 1198/5, (b) 1223/1, (c) 1248/0.25 and (d) 1273/0.25. Deformation (a–c) superplastic condition and (d) Region III behavior.

strain rate sensitivity index ($m < 0.3$ or $n = 4$–5; Figs. 7 and 8), the data from the specimen annealed at 1273 K ($d_o = 16.9$ μm) suggests the dislocation climb to be the rate controlling mechanism for deformation at elevated temperature, there appears sufficient indication of grain boundary sliding still operating. This view emerges from the observation of cavitation (Fig. 10d) along with the substantially large strain of 132% (Fig. 4) obtained in this case. Therefore, the occurrence of flow softening past the peak stress in the stress–strain curve from the coarse-grained sample (Fig. 3) can be attributed to the combined effect of particle coarsening and cavity formation by grain boundary sliding and its inadequate accommodation.

4. Summary and conclusions

High temperature constant strain rate and differential strain rate tests of the annealed specimens, with grain sizes in the range 2.9–16.9 μm, led to the following conclusions.

1. The stress–strain curves, at $\dot{\varepsilon} = 5 \times 10^{-5}\ s^{-1}$ and $T =$ 1198 K, showed flow hardening followed by flow softening. With an increase in grain size, the flow stress, in general, was found to increase and the elongation at failure was found to decrease. The maximum ductility obtained was 579%.
2. Depending on the initial grain size, high temperature deformation led to grain growth, cavitation and precipitation. In the case of fine grains, flow hardening was the result of grain growth whereas flow softening was due to cavitation. In the large grained specimen of 16.9 μm, there occurred deformation-induced precipitation and cavitation. While precipitation could cause flow hardening in the beginning, its subsequent overaging and the formation of large cavities both could cause flow softening past the peak stress.
3. log–log plot of stress and strain rate, over the strain rate range of $\sim 2.5 \times 10^{-6}$ to $3 \times 10^{-2}\ s^{-1}$ and $T = 1198$ K, exhibited superplastic region at lower strain rates with $m > 0.7$, but the same disappeared with $m \sim 0.2$ at higher strain rates. No

superplastic behavior was observed at any strain rate in the coarse grained specimen of grain size 16.9 μm.

Acknowledgements

The authors would like to thank NSERC for the financial support and Don Mardis, John Van Dorp and Mike Boskwick for the technical support.

References

[1] T.H. Courtney, Mechanical Behavior of Materials, McGraw-Hill Publishing Co. Intl. Ed., Singapore, 1990, pp. 263–324.
[2] K.A. Padmanabhan, G.J. Davies, Superplasticity, Springer-Verlag, Berlin, 1980, pp. 45–65 and 72(i)–72(iii).
[3] J.A. Wert, in: N.E. Paton, C.H. Hamilton (Eds.), Superplastic Forming of Structural Alloys, The Metallurgical Society AIME, Warrendale, 1982, pp. 69–83.
[4] B.P. Kashyap, A. Arieli, A.K. Mukherjee, J. Mater. Sci. 20 (1985) 2661–2686.
[5] V.S. Levchenko, O.V. Solovjeva, V.K. Portnoy, Y.V. Shevnuk, Mater. Sci. Forum 170–172 (1994) 261–266.
[6] F. Li, W.T. Roberts, P.S. Bate, Acta Mater. 44 (1996) 217–233.
[7] W.T. Chandler, A.K. Ghosh, W.M. Mahoney, J. Spacecraft 21 (1984) 61–64.
[8] M.W. Mahoney, in: E.A. Loria (Ed.), Superalloy 718—Metallurgy and Applications, The Minerals, Metals Mater. Soc., Warrendale, 1989, pp. 391–405.
[9] G.D. Smith, H.L. Flower, Adv. Mater. Process. 145 (1994) 37–40.
[10] B.P. Kashyap, M.C. Chaturvedi, Mater. Sci. Techno. 16 (2000) 147–155.
[11] S.J. Sijbrandij, M.K. Miller, J.A. Horton, W.D. Cao, Mater. Sci. Eng. A250 (1998) 115–119.
[12] M.K. Miller, S.S. Babu, M.G. Burke, Mater. Sci. Eng. A270 (1999) 14–18.
[13] B.P. Kashyap, A.K. Mukherjee, Res. Mech. 17 (1986) 293–355.
[14] D.S. Wilkinson, C.H. Caceres, Acta Metall. 32 (1984) 1335–1345.
[15] L. Yang, K.-M. Chang, S. Mannan, J. deBarbadillo, in: E.A. Loria (Ed.), Superalloys 718, 625, 706 and Various Derivatives, The Minerals, Metals Mater. Soc., 1997, pp. 353–365.
[16] J.R. Seidensticker, M.J. Mayo, Acta Mater. 46 (1998) 4883–4893.
[17] C. Zener quoted by C.S. Smith, Trans. Met. Soc. AIME 175 (1948) 15–51.
[18] P.K. Bakshi, B.P. Kashyap, J. Mater. Sci. 29 (1994) 2063–2070.
[19] E. Hornbogen, U. Koster, in: F. Haessner (Ed.), Recrystallization of Metallic Materials, Riederer, Stuttgart, 1978, pp. 159–194.
[20] H.J. McQueen, J.J. Jonas, in: R.J. Arsenault (Ed.), Plastic Deformation of Metals, Academic Press, New York, 1975, pp. 393–493.